Freehand system for probe-fed antenna diagnostics by means of amplitude-only acquisitions

Freehand System for Probe-Fed Antenna Diagnostics by Means of Amplitude-Only Acquisitions

Ana Arboleya, Jaime Laviada, Yuri Álvarez-López, Guillermo Álvarez-Narciandi, *Member, IEEE*, Fernando Las-Heras, *Senior Member, IEEE*, Cyril Luxey, *Fellow, IEEE*, Diane Titz, *Senior Member, IEEE*, and Aimeric Bisognin

***Abstract*— This article presents a system for easing the characterization of probe-fed antennas on available probe stations. Many of these stations were deployed for scattering parameter measurement but not for radiation pattern acquisition. Furthermore, these latter acquisitions have traditionally required the use of mechanical positioners for the automated movement of the probe antenna along different surfaces. Integration of these mechanical systems can be complex in some probe stations due to physical constraints. This work proposes an easy-to-deploy freehand system for amplitude-only field acquisitions providing great flexibility for probe-fed antenna diagnostics. In addition, the use of feeding probes, which can be bulky if compared to low-gain antennas is known to result in partial blocking avoiding the acquisition of the radiation pattern for some angles and for causing reflections yielding some ripple and distortion in the measured pattern. The system benefits from a near-field (NF) to far-field (FF) transformation based on the source reconstruction method so that unwanted reflections can be spatially identified and filtered out. Finally, broadband phaseless acquisition based on interferometry is implemented. This technique enables to alleviate the requirements of a full-vector (i.e., amplitude and phase) acquisition without losing information regarding the time-domain behavior and to retrieve all the frequencies simultaneously without losing the coherence between them so that parameters such as the delay spread can be measured. Simulated and experimental results in the V-band from 57 to 66 GHz are analyzed to validate the proposed system. Results are in fair agreement with both simulations and a direct FF acquisition on a conventional automated spherical system used as a reference.**

***Index Terms*— Amplitude-only, antenna measurement, broadband antennas, freehand system, noncontrolled environment, nonregular grids, phaseless, probe-fed antenna.**

I. Introduction

THE need for large bandwidth is moving communications to higher frequencies, involving the subsequent high compaction of the antennas. This results in many antennas being embedded on the same chip working as transmitters and/or receivers and yielding very compact devices. To characterize these compact antennas, coplanar probes are typically used. These probes enable a transition from the Vector Network Analyzer (VNA) connection in terms of waveguides or coaxial probes to coplanar (e.g., ground-signal-ground) waveguides.

Whereas the measurement of scattering parameters can be very accurate with this instrumentation, the characterization of radiation patterns becomes challenging due to: 1) the feeding probe, which can partially block the radiation from the antenna and distort the measurements [1]; 2) the positioner of the probe antenna, which has to move over the Antenna Under Test (AUT), avoiding physical contact with the feeding probe and the rest of the instrumentation (e.g., frequency extension modules, cables coming from the VNA, test bed, etc.); and 3) the use of full-acquisition schemes (e.g., vector measurements in terms of amplitude and phase), which can be expensive and, moreover, not accurate due to the phase shifting introduced by cable flexing during the movement of the equipment [2].

In order to mitigate the effect of the feeding probe, the use of custom probes has been encouraged, moving the main body far away from the antenna [1], [3] to have a minor contribution to the reflections. This is usually combined with post-processing techniques (modal filtering [3], [4] and Sources Reconstruction Method (SRM) [5]) to filter reflections from the elements surrounding the AUT.

Regarding the setups, tailored canonical ranges have been implemented [1], [3], [4], [6]. Finally, the use of phaseless techniques involving iterative schemes has been accomplished [7], though they are not appropriate for broadband antennas as they work independently for each frequency.

This article pursues to overcome the aforementioned problems in the case of probe-fed antenna measurement by using a setup based on freehand acquisitions, which avoids the use of mechanical positioners, together with a broadband interferometric setup to enable the broadband retrieval of the amplitude and phase from near-field (NF) amplitude-only acquisitions. Finally, the retrieved amplitude and phase data are used to estimate the equivalent currents on the surface of the AUT and the feeding probe so the reflections coming from the probe can be partially filtered out.

II. Freehand Measurement of Probe-Fed Antennas

The proposed system relies on three sequential steps: 1) use of the freehand acquisition system to measure the NF radiated by the AUT. This system can be easily deployed in the vast majority of probe stations; 2) phase retrieval of the measured NF by means of an interferometric technique [10]; and 3) processing of the NF amplitude by means of the SRM [8] to remove the contributions from the feeding probe.

A. Freehand Field Acquisition

In order to bypass the use of mechanical positioners, the freehand technology presented in [9] is used. It consists of tracking the probe

Manuscript received 26 September 2023; revised 22 December 2023; accepted 30 December 2023. Date of publication 1 March 2024; date of current version 6 March 2024. This work was supported in part by the Ministerio de Ciencia e Innovación of Spain (MICIN), Agencia Estatal de Investigación of Spain (AEI), and the European Union NextGenerationEU/Plan de Recuperación, Transformación y Resiliencia under Project TED2021-131975AI00/AEI/10.13039/501100011033 (ANTHEM5G); in part by MICIN, AEI, and Fondo Europeo de Desarrollo Regional (FEDER) under Project PID2021-122697OB-I00/MCIN/AEI/10.13039/501100011033 (META-IMAGER); and in part by Gobierno Principado de Asturias/FEDER under Grant AYUD/2021/51706. The Associate Editor coordinating the review process was Dr. Tae-Weon Kang. *(Corresponding author: Jaime Laviada.)*

Ana Arboleya is with the Área de Teoría de la Señal y Comunicaciones, Universidad Rey Juan Carlos, 28943 Madrid, Spain (e-mail: ana.arboleya@urjc.es).

Jaime Laviada, Yuri Álvarez-López, and Fernando Las-Heras are with the Department of Electrical Engineering, University of Oviedo, 33203 Gijón, Spain (e-mail: laviadajaime@uniovi.es; alvarezyuri@uniovi.es; flasheras@uniovi.es).

Guillermo Álvarez-Narciandi is with the Centre for Wireless Innovation, Queen's University Belfast, BT7 1NN Belfast, U.K. (e-mail: g.alvarez-narciandi@qub.ac.uk).

Cyril Luxey, Diane Titz, and Aimeric Bisognin are with the Politech' Laboratory with Politech' Lab, Université Nice Sophia-Antipolis, 06560 Valbonne, France (e-mail: cyril.luxey@unice.fr; diane.titz@univ-cotedazur.fr; aimeric.bisognin@hotmail.fr).

Digital Object Identifier 10.1109/TIM.2024.3369150

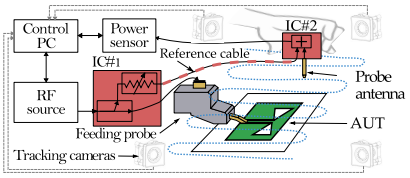

Fig. 1. Freehand acquisition system for probe-fed antennas. Two interferometric circuits IC#1 (directional coupler, variable attenuator, and reference cable) and IC#2 (power combiner) are used.

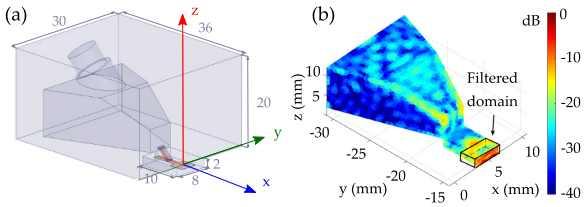

Fig. 2. (a) V-band bow tie antenna with feeding probe. (b) Reconstructed magnetic currents and filtered domain for the NF-FF transformation.

antenna (i.e., the antenna acquiring the field radiated by the probe-fed AUT), which is moved manually over the AUT to measure the radiated NF (see Fig. 1). Tracking of the measuring probe is accomplished through a motion capture system, comprising a set of at least four cameras together with specialized tracking software, and markers attached to the probe antenna. A PC is used to receive the camera data of the tracking system as well as to synchronize the VNA acquisition.

This approach is advantageous for measuring probe-fed antennas as it can be easily deployed in most of the available probe stations, even if they were intended to measure only scattering parameters since the hand movements of the probe antenna can be easily tailored to fit the available space.

B. Interferometry Field Acquisition

The time-domain interferometry in [10] is implemented to perform the phaseless measurement. This enables to retrieve coherent broadband data at each point using a single acquisition surface. The first interferometric circuit, IC#1 (see Fig. 1), takes a sample of the RF source by means of a directional coupler, which is attenuated to yield the field associated with the reference branch E_{ref}. This field, which usually is close to a narrow impulse, must be fully characterized before performing the measurements. IC#2 combines this signal and the field received from the AUT, E_{aut}, yielding the following hologram:

$$\begin{aligned} H(\vec{r},\omega) &= |E_{\text{aut}}(\vec{r},\omega)+E_{\text{ref}}(\vec{r},\omega)|^2 = |E_{\text{aut}}(\vec{r},w)|^2 \\ &\quad + |E_{\text{ref}}(\vec{r},w)|^2 + E_{\text{aut}}(\vec{r},w)\,E^*_{\text{ref}}(\vec{r},w) \\ &\quad + E^*_{\text{aut}}(\vec{r},w)\,E_{\text{ref}}(\vec{r},w) \end{aligned} \tag{1}$$

where $\vec{r}$ is the position of the probe antenna, ω denotes the angular frequency, and $*$ stands for complex conjugate. The variable attenuator pursues to match the power from both branches to avoid one masking the other. In our implementation, the combination of both signals is accomplished through a magic-T with a matched load in the 180°-shifted port.

The hologram H is modified by subtracting the squared amplitude of the reference. Then, the so-called modified hologram ($H_m(\vec{r},\omega) = H(\vec{r},\omega) - |E_{\text{ref}}(\vec{r},\omega)|^2$) is transformed to the time-domain by means of an inverse Fourier Transform (FT^{-1})

$$\begin{aligned} h_m(\vec{r},t) &= \text{FT}^{-1}\{H_m(\vec{r},\omega)\} = |e_{\text{aut}}(\vec{r},t)|^2 \\ &\quad + e_{\text{aut}}(\vec{r},t)\otimes e^*_{\text{ref}}(\vec{r},-t) + e^*_{\text{aut}}(\vec{r},-t)\otimes e_{\text{ref}}(\vec{r},t) \end{aligned} \tag{2}$$

wherein e_{aut} and e_{ref} are the inverse FT of E_{aut} and E_{ref}, respectively, and $\otimes$ denotes the convolution operator.

Since e_{ref} usually corresponds to a fixed delay through components with weak frequency dispersion (i.e., reference cable, attenuator, etc.), the corresponding signal in the time-domain is close to an impulse. Consequently, the delay of this impulse enables one to avoid the overlap of the three terms in (2). Due to that, the term $e_{\text{aut}}(\vec{r},t)\otimes e^*_{\text{ref}}(\vec{r},-t)$ can be filtered by means of time-gating. In this work a Hamming window, $W(t)$, is used [see (3)], and the complex field $E_{\text{retrieved}}$ can be retrieved back in the frequency-domain (4). A detailed study of the hologram, overlapping control, and the filtering process can be found in [10] for the case of using a radiated reference

$$h_{m\ \text{filtered}}(\vec{r},t) = h_m(\vec{r},t)\,W(t) \simeq e_{\text{aut}}(\vec{r},t)\otimes e^*_{\text{ref}}(\vec{r},-t) \tag{3}$$

$$E_{\text{retrieved}}(\vec{r},\omega) = \frac{\text{FT}\{h_{m\ \text{filtered}}(\vec{r},t)\}}{E^*_{\text{ref}}(\vec{r},\omega)} \simeq E_{\text{aut}}(\vec{r},\omega)\,. \tag{4}$$

The time-gating process defined in (3) enables to filter spurious contributions to the radiation pattern due to auxiliary elements of the setup not overlapping with the original AUT response (e.g., reflections in the walls, micro-positioner, etc.).

C. Far-Field Processing

After accomplishing the two previous steps, the complex NF at the measurement positions is available for all the frequencies of the working band. To compute the far-field (FF) the SRM [8] was chosen as it is capable of working with nonuniformly sampled domains. The SRM is based on the Electromagnetic Equivalence Principle to retrieve an equivalent current distribution on a surface enclosing the antenna and the surrounding structures, that radiate the same fields outside this surface as the enclosed elements. If the number of NF acquisition points is n and the grid is subdivided into m facets, then the equivalent currents are found by solving (5) [8]

$$\begin{bmatrix} G_J & G_m \end{bmatrix} \begin{bmatrix} J \\ M \end{bmatrix} = \begin{bmatrix} E_{\text{retrieved}} \end{bmatrix} \tag{5}$$

wherein J and M are $m \times 1$ vectors containing the complex values of the tangential components of the equivalent electric and magnetic currents on each facet, G_J and G_m are $n \times m$ matrices containing the evaluation of the Green's function relating the equivalent currents and their radiated fields at each acquisition position, and $E_{\text{retrieved}}$ is a $n \times 1$ vector containing the complex field samples.

Once the currents are found, those not corresponding to the AUT geometry are set to zero, so that only the currents characterizing the AUT are used to compute the FF.

III. Numerical Example

A V-band 5 dBi gain bow-tie antenna has been simulated together with a GSG feeding probe in HFSS for the validation of the proposed technique. The bow-tie antenna has been designed on a 0.1 mm thick silicon substrate ($\epsilon_r = 11.9$) with dimensions 4 × 3.5 mm and a feeding coplanar line of 6 mm. The feeding probe has been simulated, as shown in Fig. 2(a), considering an *Infinity Probe* from Cascade Microtech as the one employed for the experimental validation.

The surface equivalent currents have been reconstructed by means of the SRM considering the structure of the feeding probe and the AUT as shown in Fig. 2(b); then the radiation pattern is computed from a spatially filtered domain taking into account only the surface currents on the AUT [i.e., those within the filtered domain highlighted in Fig. 2(b)].

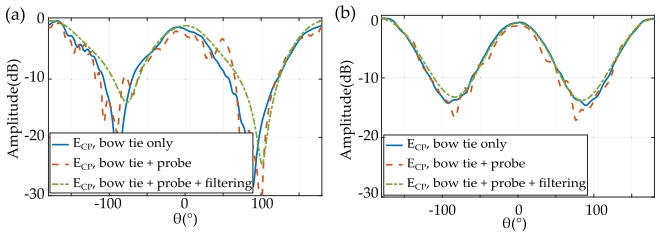

Fig. 3. Bow-tie copolar component simulated main cuts. (a) E-plane ($\phi = 0°$) and (b) H-plane ($\phi = 90°$).

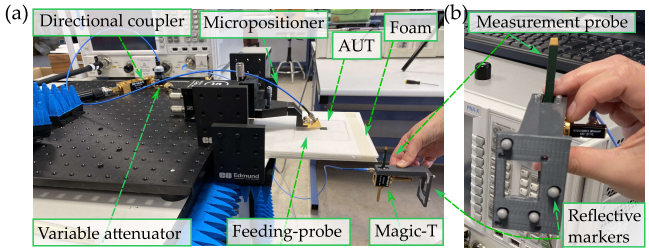

Fig. 4. Measurement setup. (a) General view and (b) measurement-probe and markers for the tracking system.

Fig. 3 shows the main cuts of the copolar component of the radiation pattern computed from the filtered currents and compared to the main cuts of a direct FF simulation of the bow-tie in both situations considering and not considering the feeding probe. The feeding probe introduces a ripple that has more effect on the plane containing the feeding probe (E-plane, $\phi = 0°$). The greater discrepancies are observed in said plane around $\theta = \pm 90°$ due to the blockage of the feeding probe. The filtering process allows to reduce those ripples and correct the effect of the feeding probe.

IV. Experimental Validation

The broadband integrated transmitter antenna for WiGig communications in the V-band working from 57 to 66 GHz consisting of a 1.1 mm square patch and a cavity, integrated within a 12 mm square Ball Grid Array (BGA), presented in [11] has been chosen for experimental validation.

The measurement setup is shown in Fig. 4(a). The AUT is oriented toward the floor so that the feeding pads (on the opposite side of the patch) are at the top to reduce the blockage of the feeding probe and the positioner. An ad hoc bracket has been manufactured for installing four optical markers within the measurement probe antenna and maximizing its visibility in the freehand acquisition process as shown in Fig. 4(b). Four tracking cameras are positioned in front of the AUT at two different heights (not shown in the pictures).

The feeding probe is a Cascade Microtech *infinity probe* as the one described in Section III and the rest of RF components for the interferometry setup described in Section II-B are: 1) a 10 dB directional coupler model 561 V-10/385; 2) a symmetrical hybrid T model 520 V/385; and 3) a variable attenuator with a 25 dB range model 635 V/385, from Mi-Wave Ltd.

To guarantee the correct acquisition of the hologram in the entire working bandwidth by means of freehand acquisitions, the intermediate frequency (IF) filter and the VNA scan time are set to the lowest possible level that provides enough dynamic range in the entire measurement domain. Conventional processing algorithms assume that each frequency scan is accomplished under static conditions, i.e., each frequency scan is performed with the probe at the same position. In order to validate that this condition is met, the position at the beginning and the end of the scan is compared. If the distance is electrically large, then that measurement is discarded. In this case,

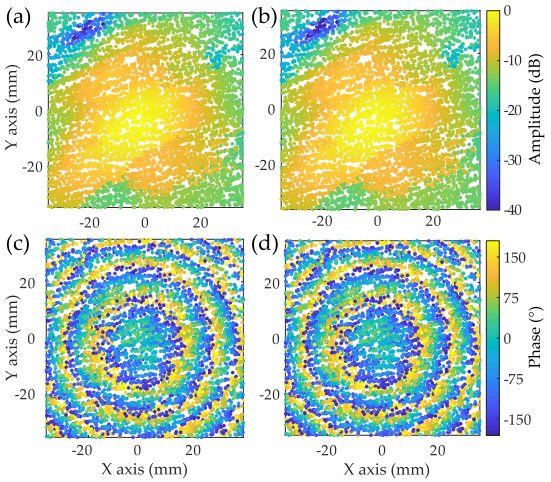

Fig. 5. Measured and retrieved E_x component at 60 GHz. (a) Measured amplitude, (b) retrieved amplitude, (c) measured phase, and (d) retrieved phase.

the distance threshold is set to 1 mm ($\sim\lambda/5$ at 60 GHz). Thus, the operator must adapt the pace to ensure the VNA performs a complete scan over an electrically small length of the scanning path. It is worth noting that the scan time can be reduced to tolerate faster speeds by increasing the IF bandwidth at the expense of reducing the signal-to-noise ratio.

NF is measured on a 7×7 cm^2 plane placed 3.5 cm below the AUT yielding a 25–30 dB drop of the field level at the edges of the acquisition plane. To minimize oversampling while fulfilling the Nyquist criterion, voxels of $\lambda/2$ at 60 GHz are considered, with a maximum of 5 samples per voxel [9]. A $\pm 5°$ limit on the measurement probe tilt is also set to make sure its pattern and polarization remain stable. The above parameters result in approximately 12 000 spatial points. 1601 frequency samples were taken in the 50–70 GHz band to avoid aliasing of the hologram [10]. The IF bandwidth was set to 100 kHz, yielding a sweep time of 23.24 ms. The acquisition time for the complete measurement was 83 min.

The retrieved amplitude and phase at 60 GHz are shown in Fig. 5 compared to the measured amplitude and phase, acquired for comparative purposes.

To quantify the quality of the phase retrieval, the metric in (6) is computed for all the frequencies yielding an error between 0.79% and 3% within the antenna working band

$$\text{error}\,(\%) = 100\frac{\|E_{\text{aut}} - E_{\text{retrieved}}\|_2}{\|E_{\text{aut}}\|_2}. \tag{6}$$

Antennas with certain directivity (like this AUT) can be characterized using only equivalent magnetic currents reconstructed on a finite aperture plane (where the tangential electric field level is significant on such plane), due to the application of the Schelkunoff's Equivalence Principle and Image Theory [12]. The equivalent magnetic currents reconstructed from $E_{\text{retrieved}}$ are shown in Fig. 6. Next, the currents within the filtered domain, encompassing the AUT, are used to calculate the FF pattern.

The main cuts of the computed FF pattern at 60 GHz are shown in Fig. 7(a) and (b) compared to the simulation and a direct FF acquisition in a spherical measurement range [7] with no post-processing. Given the size of the NF domain, the AUT, and the distance between the AUT and the acquisition plane, the FF angular margin is $\pm 45°$ [13]. The amplitude error between simulations and measurements does not exceed 4 dB within that margin. Ripples from multiple reflections are smoothed in both planes compared

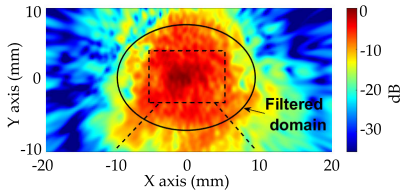

Fig. 6. Reconstructed equivalent currents in the aperture plane of the AUT. Solid line for enhancing the filtering domain and dashed lines for the position of the AUT and the feeding probe.

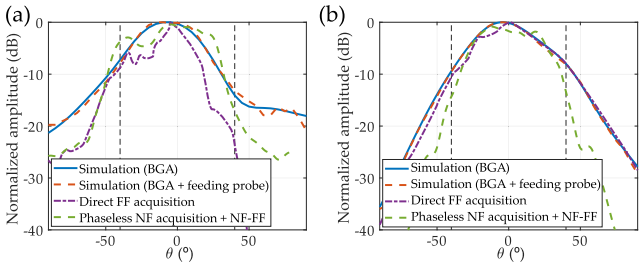

Fig. 7. Main cuts of the Copolar FF pattern at 60 GHz. (a) E-plane ($\phi = 0°$) and (b) H-plane ($\phi = 90°$). Vertical dashed lines define the valid margin of the NF-FF transformation.

to the direct FF acquisition results. In the H-plane, the phaseless results are closer to the simulation results within the valid margin of the transformation while in the E-plane, the blocking effect of the feeding-probe, and thus the distortion of the pattern, is larger. The distortion is partially compensated with the proposed method for $\theta > 0°$.

V. Conclusion

A phaseless acquisition system for broadband probe-fed antennas based on freehand arbitrary NF acquisitions is presented. Freehand acquisition is based on an optical tracking system that provides sub-mm accuracy. The phase is retrieved at each spatial acquisition point coherently for all the frequencies by means of an interferometric scheme. Next, an SRM is employed to compute the equivalent currents and FF pattern at each frequency from the arbitrary NF grid data. Time and spatial filtering are applied in the post-processing stage in order to minimize the effect of the feeding-probe and surrounding elements. Since the phase is retrieved coherently at each acquisition point, the proposed system and techniques can be adapted to different acquisition domains and further post-processing in such a way that group delay computation can be performed from phaseless NF acquisitions. Validation results are presented for a V-band WiGig antenna showing an acceptable agreement with simulations and direct spherical FF acquisition. Larger acquisition planes or other evolving geometries are expected to improve the results and can be implemented thanks to the flexibility of the proposed freehand system, at the expense of increasing aquisition time. The quality of results is comparable to that obtained with in-house dedicated and automated FF acquisition systems. The proposed system can be employed in new cost-effective probe-fed antenna measurement systems or to extend the functionality of conventional probe stations for scattering parameter measurement.

References

[1] A. C. F. Reniers, A. R. van Dommele, A. B. Smolders, and M. H. A. J. Herben, "The influence of the probe connection on mm-wave antenna measurements," *IEEE Trans. Antennas Propag.*, vol. 63, no. 9, pp. 3819–3825, Sep. 2015.

[2] D. J. van Rensburg, "A technique to evaluate the impact of flex cable phase instability on mm-wave planar near-field measurement accuracies," ESA ESTEC, Noordwijk, The Netherlands, Rep. WPP-164, 1999.

[3] L. Böhm, "Measurement techniques for highly integrated mm-wave antennas," Ph.D. dissertation, Institut für Mikrowellentechnik, Ulm, Germany, 2019.

[4] E. C. Lee, E. Szpindor, and W. E. McKinzie III, "Mitigating effects of interference in on-chip antenna measurements," in *Proc. AMTA 37th Annu. Meeting Symp.*, Long Beach, CA, USA, Oct. 2015, pp. 445–450.

[5] L. J. Foged, L. Scialacqua, P. Iversen, and E. Szpindor, "Detection and suppression of scattered fields from coplanar micro-probe and positioner in millimeter wave on-chip antenna measurements," in *Proc. Int. Symp. Antennas Propag. (ISAP)*, Oct. 2016, pp. 126–127.

[6] D. Titz, F. Ferrero, and C. Luxey, "Development of a millimeter-wave measurement setup and dedicated techniques to characterize the matching and radiation performance of probe-fed antennas [measurements corner]," *IEEE Antennas Propag. Mag.*, vol. 54, no. 4, pp. 188–203, Aug. 2012.

[7] A. Bisognin et al., "Ball grid array module with integrated shaped lens for 5G backhaul/fronthaul communications in F-band," *IEEE Trans. Antennas Propag.*, vol. 65, no. 12, pp. 6380–6394, Dec. 2017.

[8] Y. Alvarez, F. Las-Heras, and M. R. Pino, "Reconstruction of equivalent currents distribution over arbitrary three-dimensional surfaces based on integral equation algorithms," *IEEE Trans. Antennas Propag.*, vol. 55, no. 12, pp. 3460–3468, Dec. 2007.

[9] G. Álvarez-Narciandi, J. Laviada, Y. Álvarez-López, and F. Las-Heras, "Portable freehand system for real-time antenna diagnosis and characterization," *IEEE Trans. Antennas Propag.*, vol. 68, no. 7, pp. 5636–5645, Jul. 2020.

[10] A. Arboleya, J. Laviada, J. Ala-Laurinaho, Y. Álvarez, F. Las-Heras, and A. V. Räisänen, "Phaseless characterization of broadband antennas," *IEEE Trans. Antennas Propag.*, vol. 64, no. 2, pp. 484–495, Feb. 2016.

[11] A. Bisognin et al., "Low-cost organic-substrate module for Tx–Rx short-range WiGig communications at 60 GHz," *IEEE Trans. Antennas Propag.*, vol. 69, no. 10, pp. 6196–6208, Oct. 2021.

[12] S. R. Rengarajan and Y. Rahmat-Samii, "The field equivalence principle: Illustration of the establishment of the non-intuitive null fields," *IEEE Antennas Propag. Mag.*, vol. 42, no. 4, pp. 122–128, Aug. 2000.

[13] *IEEE Recommended Practice for Near-Field Antenna Measurements*, IEEE Standard 1720-2012, Dec. 2012, pp. 1–102.